ISSN : 0974 - 7486 Volume 14 Issue 1

Materials Science

An Indian Journal

Full Paper

MSAIJ, 14(1), 2016 [023-031]

Measurement of microstructural defect parameters in tungsten dichalcogenides: useful materials for the Li-ion battery applications

T.K.Mandal*, G.Bhoj

Faculty of Science and Technology, The ICFAI University, Rajawala Road, Central Hope Town, Selaqui, Dehradun-248197, Uttarakhand, (INDIA)

E-mail: tapanm@yahoo.com

ABSTRACT

Microstructural defect parameters like crystallite size (P), dislocation density (ρ), rms strain $(\langle e^2 \rangle)^{1/2}$, stacking fault probability (α), fractional change in interlayer spacing (g) and proportion of the plane affected by defects (γ) are evaluated with the help of X-ray diffraction (XRD) studies for tungsten sulphoselenide, $WS_{2-x}Se_x$ ($0 \le x \le 2$) compounds. These structural defect parameters are correlated with the compositional changes. The variation of conductivity with composition have also been correlated in terms of the structural defect parameters like P, ρ, $(\langle e^2 \rangle)^{1/2}$, α, g and γ. Room temperature electrical conductivity measurements indicated the semiconduction behavior in $WS_{2-x}Se_x$($0 \le x \le 2$) compounds. Microstructural defect parameters are corelated with the electrical conductivities.

KEYWORDS

Tungsten sulphoselenide;
Microstructural defect parameters;
Electrical conductivity.

INTRODUCTION

Layered transition metal dichalcogenides (TMDs), MX_2 (M = Mo, W; X = S, Se), have been the subject of a great deal of investigation in the recent years[1-8]. TMDs are anisotropic materials having strong bonding within the layers and weak van der waals interactions in between the layers[9-12]. Tungsten disulfide (WS_2), as a typical TMD[13], has garnered spectable interest for its unusual combination of properties and extensive applications in catalysis, photosensor devices, field-effect transistors, hydrosulfurization, hydrogen evolution reactions, tribological applications and lubricants[2-7,10-11,13]. The graphene-like layered material WS_2 has been attracted great attention as promising anode materials for lithium ion batteries (LIBs) because of their unique layered crystal structure, which prefers ions and molecules for the intercalation[14]. The underlying crystal structure of WS_2 is composed of three stacked atom layers S-W-S held together by van der Waals forces and is beneficial to sustain fast insertion/de-insertion of Li+ ion[4-7,14]. The graphene-like layered material WS_2 has higher theoretical capacity (433 $mAhg^{-1}$) than that of commercial graphite (372 $mAh\ g^{-1}$)[14].

A significant amount of work on WS_2 and TMDs has been reported by a number of researchers[1-14]. Hwang et[1] al reported room temperature modulation and ambipolar behavior of layered semiconduc-

tor WS_2 in the transistor application. Wang and coworkers[2] developed the WS_2-based counter electrodes for the dye-sensitized solar cells. Synthesis and electrochemical performances of layered tungsten sulfide-graphene nanocomposite as a sensing platform for catechol, resorcinol and hydroquinone have been reported by Huang et al[3]. Pumera and Loo[4] employed TMD (MoS_2 and WS_2) materials for sensing and biosensing devices. Zonghua et al[5] found WS_2 as promising candidates for replacing noble metal catalysts due to their inexpensive cost and good electrocatalytic activities towards the hydrogen evolution reaction. MoS_2 and WS_2 nano objects have been studied in tribological applications by Maharaj and Bhushan[6]. A fundamental study on the effects of exfoliation on the inherent electrochemical properties of TMD (MoS_2, $MoSe_2$, WS_2, WSe_2) materials have been carried out by Loo et al[7]. Measurement of high exciton binding energy in the monolayer transition metal dichalcogenides WS_2 and WSe_2 have been investigated by Hanbicki and coworkers[8].

Bhandavat and Fang et al investigated different morphologies and sizes of WS_2 as anode materials for LIBs[15–16]. Fang et al observed that the morphology of the as prepared WS_2 depends with the W/S ratio[16]. They, with the X-ray absorption near-edge structure characterization showed that the d electrons of W deviate towards the Li (or S) atom during the discharge/ charge process, thereby forming a weak bond between W and Li_2S (or S)[16]. In order to avoid the disadvantages of rapid decay of capacity and poor rate capability of the W-S-W stacking sheets and low electronic conductivity in TMDs, Chen et al introduced a conductive spacer between WS_2 nanosheets through an efficient route[17]. Wang et al. reported that layered MoS_2 intercalated by single-wall carbon nanotubes (SWCNT) can improve both stability and discharge capacity[18]. A new composite consisting of graphene, poly ethylene oxide and exfoliated MoS_2, which showed high sepcific capacity and excellent high-rate performance for reversible Li^+ storage, was designed by Xie and coworkers[19]. Liu et al confirmed that the connectivity of intercalation of SWCNT and CuO in WS_2, with the discharge and charge specific capacities and electrochemical reversibilities of LIBs, are associated with the structural stability of the electrode materials[20]. The degradation of the specific capacities of $LiMn_2O_4$ spinel, a promising candidate as cathode material in LIBs, was attributed to lattice defects[21] by Kaiya et al. By constructing a simple Sn–Li battery system, Hirai et al investigated the effects of the volume change associated with the formation of Li–Sn compounds on the electrode potential from the viewpoint of the Gibbs free energy and associated elastic-strain energy[22]. Wei group investigated the doping of atomic vacancies in the monolayers of tungsten disulfide by density functional theory calculations[23]. Their results revealed that the atomic vacancy defects affect the electronic and optical properties of the tungsten disulfide monolayers. The strongly ionic character of the W-S bonds and the nonbonding electrons of the vacancy defects result in spin polarization near the defects.

Despite of all these recent progresses on the TMD (MoS_2, $MoSe_2$, WS_2, WSe_2) materials, there are many gaps in our understanding of the fundamental interactions which lead to the striking optical and electronic properties of these semiconducting materials. One very important espect of these materials are defect properties like crystallite size, rms strain, dislocation density, stacking faults, fractional change in interlayer spacing and the proportion of the planes affected by defects, which profoundly influence the electronic and optical properties of these materials. Very less work has been explored with these issues on WS_2 and $WS_{2-x}Se_x(0\leq x\leq 2)$ materials. However, these defect properties of WS_2 and $WS_{2-x}Se_x(0\leq x\leq 2)$ play a vital role in governing their suitability in the derired applications. The present paper addresses the X-ray line profile analysis of $WS_{2-x}Se_x(0\leq x\leq 2)$ compounds in order to investigate the crystallite size, rms strain, dislocation density, stacking fault probability, fractional change in interlayer spacing and proportion of the plane affected by defects.

EXPERIMENTAL DETAILS

The $WS_{2-x}Se_x(0\leq x\leq 2)$ compounds were synthesized directly from the elements and the method of preparation is similar as reported earlier[11]. Appro-

priate amounts of the powdered elements were weighed accurately to produce the desired composition, mixed intimately to prepare a homogenous mixture, placed inside a quartz tube, which was sealed in vacuum and placed inside a furnace. The powder mixtures were heated slowly up to 400^0C and kept for 72 h followed by heating at 750^0C for 48 h and finally at 1000^0C for 40 h. Then, the furnace was slowly cooled down to room temperature.

In order to measure the XRD the ingots were ground properly at room temperature. XRD of these powdered samples were carried out on a Philips 1729 diffractometer using monochromatic CuK$\alpha_?$ radiation. Accurate lattice parameters were obtained by the least square method. Earlier studies on the effect of crystallite size by the line profile of WS_2 have shown that the crystallite size affects the low - angle region of the profile whereas the high angle region remained unchanged. The intensity profiles of the (002) reflection in the X-ray diffractograms of all the samples were recorded from which structural parameters like dislocation density, root mean square strain and layer disorder parameters were calculated adopting a single line technique similar to that described earlier[11].

The physical significance of variance or the second moment about the mean, defined by

$$W = \frac{\int(\theta - \bar{\theta})^2 I(\theta)d\theta}{\int I(\theta)d\theta}$$

as a measure of line broadening due to crystallite size, strain, mistake and dislocations. Here θ is the diffraction angle, $\bar{\theta}$ is the centroid of X-ray line profile, I(θ) is the diffracted intensity at θ. Based on this variance of the line profile, $W(2\theta)$, can be written as[9,10]

$$W(2\theta) = \frac{\lambda\Delta(2\theta)}{2\pi^2 P_V \cos\theta} + \frac{S\lambda^2}{\cos^2\theta}$$

where $S = \frac{< e^2 > -\beta_d{}^2/\pi^2}{d^2}$

$\Delta(2\theta)$ is the angular range over which the intensity distribution is applicable, $<e^2>$ is the mean square strain, λ is the wavelength of the X-rays, θ is the Bragg angle and d is the interplanar distance. P_V is the apparent crystallite size, which is obtained by the method of variance. The true crystallite size as determined by the method of Fourier analysis[9], P_F and P_V are related as

$$\frac{1}{P_V} = \frac{1}{P_F} + \frac{\beta_d}{d}$$

where β_d is the integral width of the defect profile. Thus a plot of $W(2\theta)$ as ordinate versus $\Delta(2\theta)$ as abscissa by emphasizing the points corresponding to the tail, will be linear and the slope will give apparent crystallite size P_V and the intercept, $(< e^2 > -\beta_d{}^2/\pi^2)/(\lambda^2/\cos^2\theta$. Thus knowing the values of P_F and P_V the value of β_d can be obtained. The magnitudes of mean fractional change in the inter layer distance g in the direction of d_{002} and the fractions (γ) of the planes affected by layer disorders have been calculated according to the expressions used as follows[11]:

$$g = \frac{1}{\pi l}\cot^{-1}\left(\frac{\pi\Delta}{\beta_d}\right)$$

$$\gamma = \frac{\beta_d}{\sin^2(\pi.l.g)}$$

where, l is the order of reflection, Δ is the measure of peak shift from the centroid of the diffraction profile. A dislocation is an imperfection in a crystal associated with the misregistry of the lattice in one part of the crystal with that in another part. The dislocation density (ρ) has been estimated[25] using the relation

$$\rho = \frac{2(3 < e^2 >)^{1/2}}{bP_V}$$

where b is the Burger's vector.

Warren[10] defined stacking fault probability (α) as probability of finding a deformation between any two successive layers. The average number of layers between faults is $1/\alpha$ assuming that the probability of a fault between any two layers is independent of the faulting between other layers. Thus α can be calculated using

$$-\left(\frac{dA_n}{dn}\right) = \frac{1}{P_V} + \frac{3\alpha ld}{c^2}$$

where $\left(\frac{dA_n}{dn}\right)$ is the initial slope of the Fourier coefficient (A_n) obtained from Fourier analysis of X-ray

diffraction profile versus order (n)[10], c is the lattice parameter in the direction of stacking and *l* the order of reflection.

The crystallite size anisotropy (P_F^{002}/ P_F^{103}) for all these compounds was calculated by finding out the relative change in the true crystallite size (P_F) for 002 and 103 reflections. Room temperature electrical conductivity measurements were performed using a two probe method on compressed pellets. The compressed samples may involve oxidation barriers between the particles and some voids. Existence of air holes may also strongly affect the electrical properties. Therefore all the electrical measurements have been performed on sintered pellets.

RESULT AND DISCUSSION

Figure-1 shows the X-ray diffractograms (XRD) of $WS_{2-x}Se_x$ ($0 \le x \le 2$) compounds. The XRD of $WS_{2-x}Se_x$($0 \le x \le 2$) compounds were thoroughly scanned for all the possible phases e.g., WS_2, WSe_3, W_3Se_4 etc. The peaks observed in the diffractogram in Figure 1(a) are assigned in terms of Miller-indices (hkl) considering a hexagonal crystal structure (space group $P6_3/mmc$) with the lattice parameters a = 0.315 nm and c = 1.235 nm[26-27]. The diffractograms in Figure 1 for $WS_{2-x}Se_x$ ($0 \le x \le 2$) compounds showed good resemblance with one another, suggesting that even upon selenium substitution in WS_2, the structure of the host remains unchanged. The inter planer distance calculations corresponding to different planes are found to be in good agreement with the reported data[26-27]. The most intense peak (relative intensity = 100%) lies at 0.6162 nm in (002) reflection. The maximum intensity of the (002) reflection indicates a strong orientation along the c-axis. The other (00*l*) reflections such as (004), (006) and (008) are of relatively much weaker intensity. The intensity variation for (100), (10l) and (11l) reflections do not show any definite trend towards composition for $WS_{2-x}Se_x$($0 \le x \le 2$) compounds. The lattice parameters (a and c) of all these compounds well match with that of the reported lattice parameters on $WS_{2-x}Se_x$($0 \le x \le 2$) compounds[28-30]. Figure 2A and 2B presents a schematic variation of lattice parameters (a and c) and a/c respectively with composition (x) for

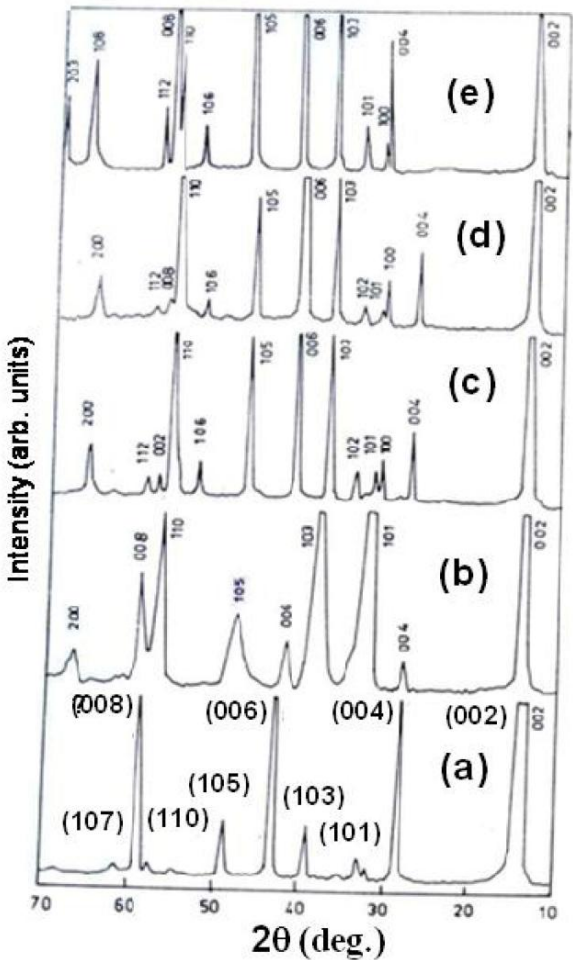

Figure 1 : X-ray diffractogram of (a) WS_2 (b) $WS_{1.5}Se_{0.5}$ (c) $WS_{1.0}Se_{1.0}$ (d) $WS_{0.5}Se_{1.5}$ and (e) WSe_2 compounds

$WS_{2-x}Se_x$($0 \le x \le 2$) compounds. It shows that both a and c varies linearly with the composition. The variation of c/a with composition shows a maximum for $WS_{1.0}Se_{1.0}$ compound almost similar to as reported by Mentzen and Sienko[28].

Figure 3 shows the crystallite sizes of $WS_{2-x}Se_x$($0 \le x \le 2$) compounds calculated on the basis of variance (P_V) as well as Fourier methods (P_F). Figure 3 indicates a lower value of crystallite size (P_V), calculated by the variance method, as compared to that of the Fourier method (P_F). Such a difference may be attributed to the fact that the size obtained by Fourier method represents the volume average of the crystallite-dimensions measured normal to the reflecting planes, whereas in the case of variance method, it is a measure of mean thickness given by E = V/A, where A is the area of the projection of the crystallite of volume V on the reflecting plane and

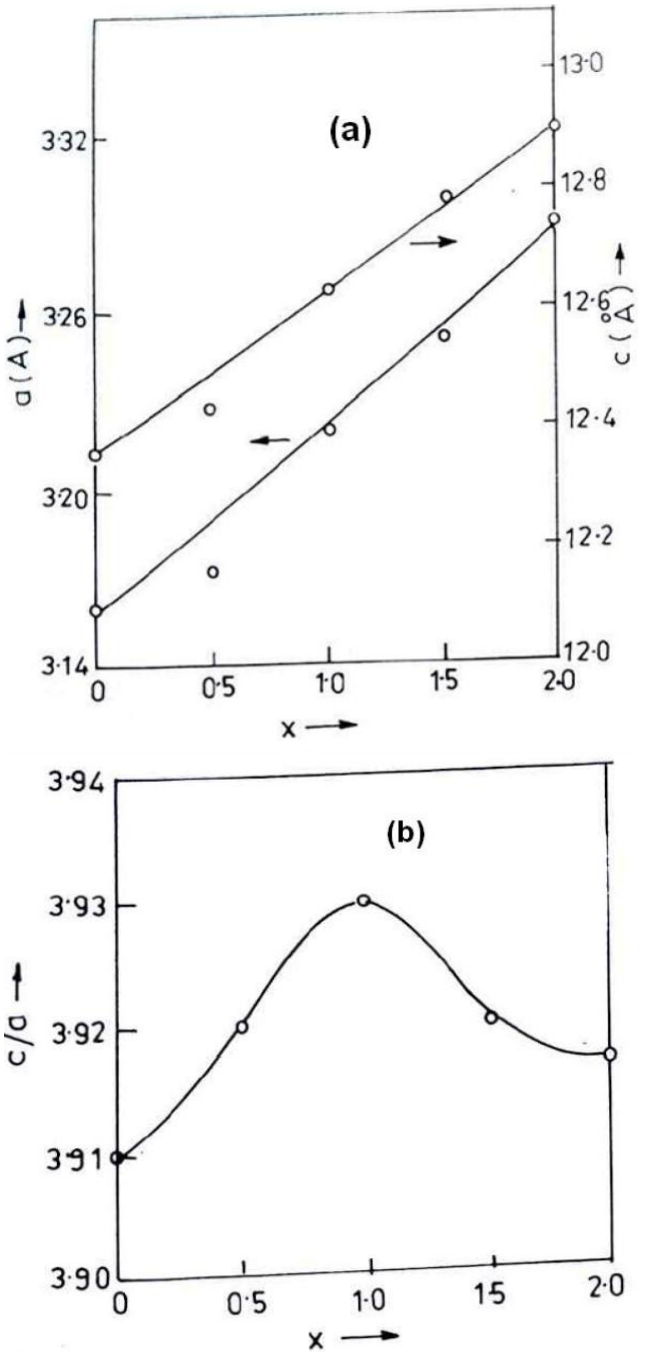

Figure 2 : Variation of (a) lattice parameters (a and c) and (b) c/a with composition (x) for $WS_{2-x}Se_x$ ($0 \le x \le 2$) compounds

is dependent on the defect concentrations[31]. It appears from the data here that the size of the crystalite reaches a maximum value when the composition of sulphur and selenium is identical, ie. $WS_{1.0}Se_{1.0}$. In other compounds, with sulphur reach and selenium deficiency or vice versa, a decrease in the crystallite size is observed. In addition to the imperfection of the crystallites as well as of lattice strain, dislocation and stacking faults are known to cntribute towards the broadening of X-ray lines. Therefore the extent of intensity spread for each specimen is a measure of the nature and extent of lattice imperfections. Assuming that the defects are not related to each other, root mean square displacements ($<e^2>^{1/2}$) and dislocation density (ρ) were calculated by variance method for (002) reflection in $WS_{2-x}Se_x$ ($0 \le x \le 2$) compounds. It is noted that with increasing selenium content in $WS_{2-x}Se_x$ ($0 \le x \le 2$) compounds both ($<e^2>^{1/2}$) and ρ decrease [Figure 4] gradually and attain a lowest value for $WS_{1.0}Se_{1.0}$ and thereafter it showed an incresing trend. Such a behavior is just opposite to as observed in variation of crystallite size with composition. It is to be noted that the crystallite size values as determined by X-ray line profile analysis is the size of the crystallites which is surrounded by grain bondaries at the interfaces. With increase in the crystallite size value, the ratio of number of atoms lying in the grain boundaries region is smaller. Since the grain boundaries are formed by dislocation networks which also gives rise small inhomogenious strain, it is expected that the ($<e^2>^{1/2}$) and ρ values decrease with composition (x) and attain a minima at $WS_{1.0}Se_{1.0.}$ Thus when

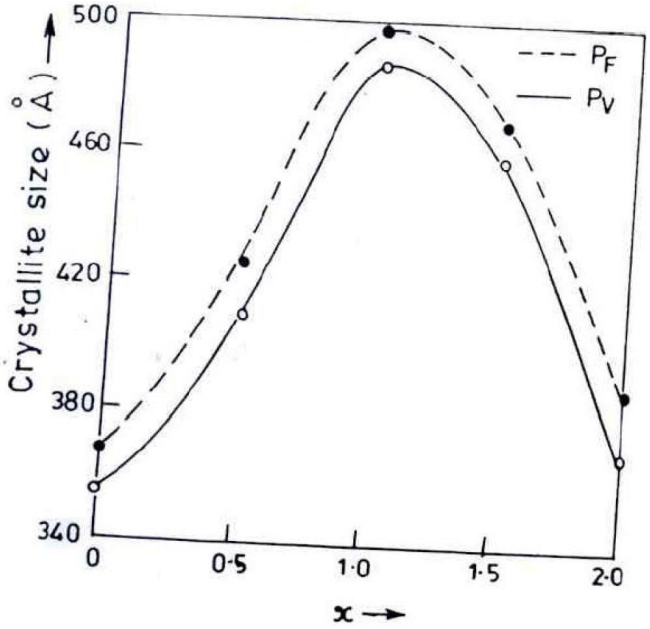

Figure 3 : Variation of the crystallite size of $WS_{2-x}Se_x$ ($0 \le x \le 2$) compounds by variance (P_V) and Fourier (P_F) techniques

Full Paper

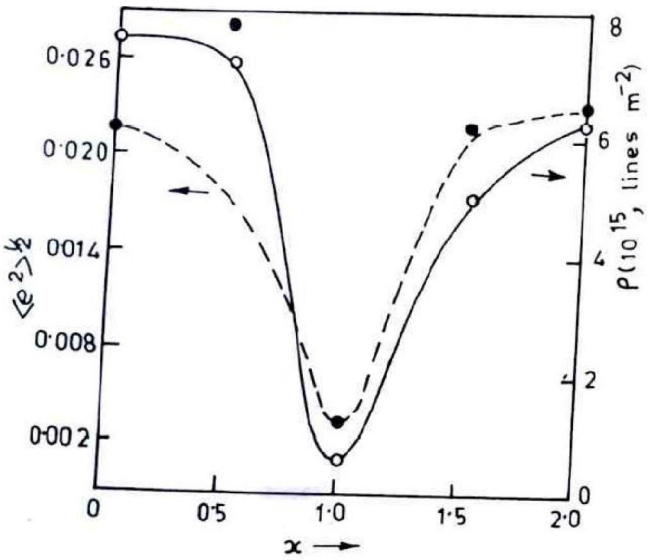

Figure 4 : Variation of rms strain ($<e^2>^{1/2}$) and dislocation density (ρ) of $WS_{2-x}Se_x$ (0≤x≤2) compounds

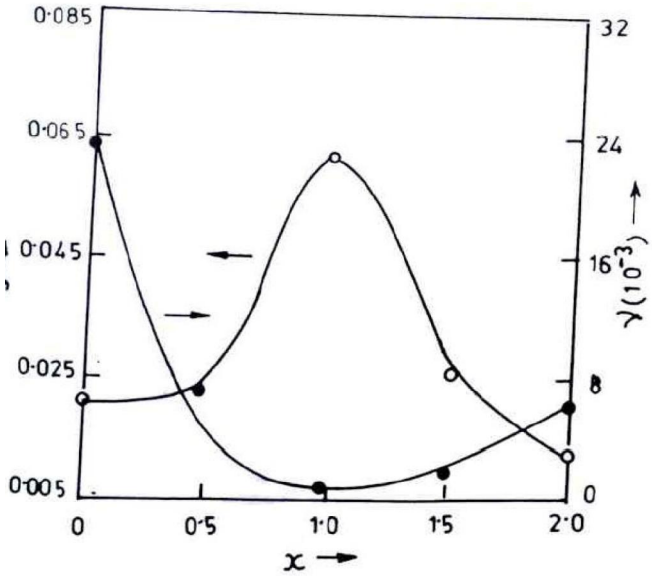

Figure 5 : Variation of fractional change in interlayer spacing (g) and proportion of the plane affected by defects (γ) for $WS_{2-x}Se_x$ (0≤x≤2) compounds

the sulphur and selenium are in the same proportion, strains are released more i.e more ordering is introduced in the sample. Any deviation from the composition introduced large amound of chaos. This is possibly due to breaking of the crystallites which leads to the corresponding increase in the rms strain as well as the dislocation density.

Figure 5 shows the variation of inter layer spacing (g) and the fractions of the planes affected by defects (γ). It is obvious that g showed behavior just opposite to the crystallite size and with composition in $WS_{2-x}Se_x$(0≤x≤2) compounds. It showed the presence of maxima at $WS_{1.0}Se_{1.0}$ suggesting thereby the presence of maximum layer disorder in this compound. It is also seen from the figure that γ in WS_2 is relatively much higher than that of WSe_2. It is also noted that γ decreases very rapidly up on slenium substitution in WSe_2 and attains a minima at $WS_{1.0}Se_{1.0}$ and then it is slightly improved. This could be explained in terms of van der Waals forces which are operating in between the chalcogen layers. Since the van der Waals forces in between two selenium layers is much stronger than for the layers containing sulphur. Thus the probability of the planes affected by defects will increase as the amount of sulphur increases in $WS_{2-x}Se_x$(0≤x≤2) compounds.

The variation of crystalite size anisotropy (P_F^{002}/ P_F^{103}) and stacking fault probability (α) for $WS_{2-x}Se_x$(0≤x≤2) compounds are displayed in Figure 6.

It is observed that both showed almost similar trend in their behavior. Initially both α and P_F^{002}/ P_F^{103} increased almost linearly with composition (x) upto $WS_{1.0}Se_{1.0}$ and then decreased upto WSe_2. The exact reason for the crystallite size anisotropy in measurements with polycrystalline aggregates is hard to found. Even if there exists a real crystallite shape anisotropy, this will be blurred the random orientation of the crystallites if all possible orientations

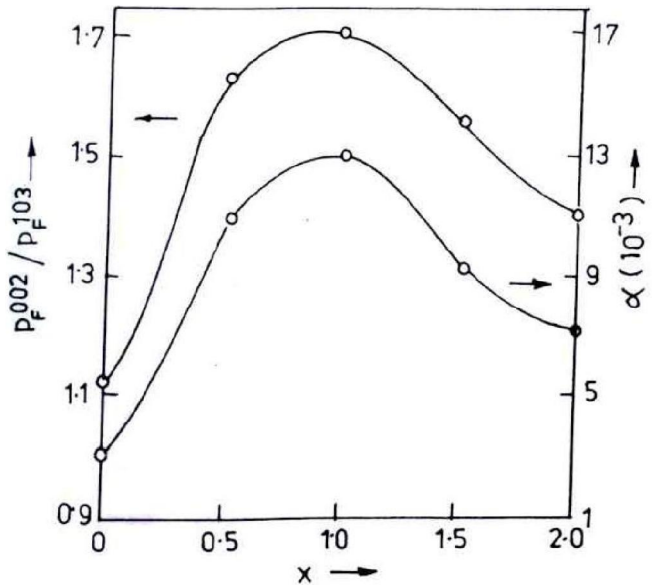

Figure 6 : Variation of crystallite size anisotropy (P_F^{002}/ P_F^{103}) and stacking fault probability (α) for $WS_{2-x}Se_x$ (0≤x≤2) compounds

TABLE 1 : Magnetic and electrical data of $WS_{2-x}Se_x$ ($0 \le x \le 2$) compounds

Compounds	$-\chi_g \times 10^{-6}$	Conductivity type	σ_{300K} (mho cm^{-1})
WS_2	0.35	p	2.0×10^{-4}
$WS_{1.5}Se_{0.5}$	0.31	p	2.7×10^{-5}
$WS_{1.0}Se_{1.0}$	0.28	p	1.4×10^{-6}
$WS_{0.5}Se_{1.5}$	0.17	p	1.0×10^{-5}
WSe_2	0.08	n	2.0×10^{-4}

have equal probability of occurence. If, however, there is a slight preference of some orientation, the average size in one direction may be different from other direction. The other reason for apparent crystallite size anisotropy may be due to the occurrence of stacking faults. As has been shown by Warren et al[32] and Wagner et al[33] the X-ray diffraction broadening of (111) and (200) reflections of FCC polycrystals are affected differently by the presence of stacking faults and the apparent crystallite sizes are different in two directions. The fact that crystallite size anisotropy as observed in thr present investigation is almost invariably accompanied by stacking faults indicates that preffered orientation plays an important role in giving rise this anisotropy. It appears from this data that the increasing faulting type introduced the breaking of crystallites in a particular direction. This may lead to the crystallite size anisotropy as observed in the $WS_{2-x}Se_x$($0 \le x \le 2$) systems. Thus based on observations from Figure 6 for α and P_F^{002}/P_F^{103} respectively it is interesting to note that whenever α is low the size in that direction (P_{001}) is high and vice versa.

Room temperature thermoelectric power measurements indicated that WS_2 and $WS_{2-x}Se_x$($0 \le x \le 2$) compounds possess p and n type conductivity respectively. The room temperature conductivity (σ_{300K}) data in TABLE 1 shows that σ in case of solid solution formation has decrease to some extent in comparison to pure MoS_2 and $MoSe_2$. These studies confirmed the semiconducting behavior of $WS_{2-x}Se_x$($0 \le x \le 2$) compounds.

CONCLUSIONS

X-ray line profile analysis has been carried out in order to estimate the microstructural defects like crystallite size (P), dislocation density (ρ), rms strain ($\langle e^2 \rangle^{1/2}$), stacking fault probability (α), fractional change in interlayer spacing (g) and proportion of the plane affected by defects (γ) for $WS_{2-x}Se_x$($0 \le x \le 2$) compounds. It has been observed that P, ($\langle e^2 \rangle^{1/2}$, γ and ρ are lowest for $WS_{1.0}Se_{1.0}$ while g, α and P_F^{002}/P_F^{103} showed a reverse trend. It is thereby concluded that the microstructural defects are relatively low in $WS_{1.0}Se_{1.0}$ and deviation from this composition in $WS_{2-x}Se_x$($0 \le x \le 2$) introduces more values of g, α and P_F^{002}/P_F^{103} and less values of P, ($\langle e^2 \rangle^{1/2}$, γ and ρ. Room temperature electrical conductivity measurement indicated the lowest conductivity value in $WS_{1.0}Se_{1.0}$ in comparison to other compounds in $WS_{2-x}Se_x$($0 \le x \le 2$). Thus the microstructural defect parameter calculations and their corelation with the electrical property of $WS_{2-x}Se_x$($0 \le x \le 2$) can guide the desired electrochemical properties of WS_2 based compounds for its applications in the Li ion battery.

REFERENCES

[1] W.S.Hwang, M.Remskar, R.Yan, V.Protasenko, K.Tahy, S.D.Chae, P.Zhao, A.Konar, H.Xing, A.Seabaugh, D.Jena; "Transistors with chemically synthesized layered semiconductor WS_2 exhibiting 10^5 room temperature modulation and ambipolar behavior", *Applied Physics Letters*, **101**, 013107 **(2012)**.

[2] Y.Wang, S.Li, Y.Bai, Z.Chen, Q.Jiang, T.Li, W.Zhang; "Dye-sensitized solar cells based on low cost carbon-coated tungstendisulphide counter electrodes", *Electrochimica Acta*, **114**, 30– 34 **(2013)**.

[3] K.J.Huang, L.Wang, Y.J.Liu, T.Gan, Y.M.Liu, L.L.Wang, Y.Fan; "Synthesis and electrochemical performances of layered tungstensulfide-graphene nanocomposite as a sensing platform for catechol, Resorcinol and hydroquinone", *Electrochimica Acta*, **107**, 379– 387 **(2013)**.

[4] M.Pumera, A.H.Loo; "Layered transition-metal dichalcogenides (MoS_2 and WS_2) for sensing and biosensing", *Trends in Analytical Chemistry*, **61**, 49–53 **(2014)**.

[5] Z.Pu, Q.Liu, A.M.Asiri, A.Y.Obaid, X.Sun; "One-step electrodeposition fabrication of graphene film-confined WS_2 nanoparticles with enhanced electrochemical catalytic activityfor hydrogen evolution", *Electrochimica Acta*, **134**, 8–12 **(2014)**.

[6] D.Maharaj, B.Bhushan; "Characterization of nano friction of MoS_2 and WS_2 nanotubes", *Materials Letters*, **142**, 207–210 **(2015)**.

[7] A.H.Loo, A.Bonanni, Z.Sofer, M.Pumera; Exfoliated transition metal dichalcogenides (MoS_2, $MoSe_2$, WS_2, WSe_2): An electrochemical impedance spectroscopic investigation", *Electrochemistry Communications*, **50**, 39–42 **(2015)**.

[8] A.T.Hanbicki, M.Currie, G.Kioseoglou, A.L.Friedman, B.T.Jonker; "Measurement of high exciton binding energy in the monolayer transition metal dichalcogenides WS_2 and WSe_2", *Solid State Communications*, **203**, 16–20 **(2015)**.

[9] S.K.Srivastava, T.K.Mandal, B.K.Samantaray; "Studies on layer disorder, Microstructural parameters and other properties of tungsten substituted molybdenum disulphide, $Mo_{1-x}W_xS_2$ (0 x 1)", *Synthetic Metals*, doi:10.1016/S0379-6779(97)81262-3, **90(2)**, 135-142 **(1997)**.

[10] T.K.Mandal, S.K.Srivastava, B.K.Samantaray, B.K.Mathur; "Structural characterization of indium intercalation compounds of molybdenum sulphoselenide by X-ray diffraction and electron microscopy", *Journal of Materials Scence Letters*, Doi:10.1023/A:1006644109823, **18(11)**, 859-864 **(1999)**.

[11] T.K.Mandal, S.K.Srivastava, B.K.Samantaray, B.K.Mathur; "X-ray diffraction and electron microscopic studies on selenium substituted indium intercalation compounds of tungsten disulphide", *Materials Science & Engineering B*, doi:10.1016/S0921-5107(99)00169-5, **64(3)**, 143-148 **(1999)**.

[12] T.K.Mandal, S.K.Srivastava, P.Bala, B.K.Samantaray, B.K.Mathur; "X-ray diffraction and scanning tunnelling microscopic studies of indium intercalation compounds of tantalum disulphide and diselenide", *Indian Journal of Physics*, **74A**, 453 **(2000)**.

[13] S.Cao, T.Liu, S.Hussain, W.Zeng, X.Peng, F.Pan; "Hydro thermal synthesis of variety low dimensional WS_2 nanostructures", Materials *Letters*, **129**, 205–208 **(2014)**.

[14] W.Lv, J.Xiang, F.Wen, Z.Jia, R.Yang, B.Xu, D.Yu, J.He, Z.Liu; "Chemical vapor synthesized ws_2-embedded polystyrene-derived porous carbon as superior long-term cycling life anode material for li-ion batteries", *Electrochimica Acta*, **153**, 49–54 **(2015)**.

[15] R.Bhandavat, L.David, G.Singh; "Synthesis of Surface-Functionalized WS_2 Nanosheets and Performance as Li-Ion Battery Anodes", *The Journal of Physical Chemistry Letters*, doi:10.1021/jz300480w, **3(11)**, 1523–1530 **(2012)**.

[16] X.P.Fang, C.X.Hua, C.R.Wu, X.F.Wang, L.Y.Shen, Q.Y.Kong, J.Z.Wang, Y.S.Hu, Z.X.Wang, L.Q.Chen; "Synthesis and electrochemical performances of graphene-like WS_2", *Chem.Eur.J.*, **19**, 5694–5700 **(2013)**.

[17] D.Y.Chen, G.Ji, B.Ding, Y.Ma, B.H.Qu, W.X.Chen, J.Y.Lee; "In situ nitrogenated graphene-few-layer WS_2 composites for fast and reversible Li+ storage", *Nanoscale*, **5(17)**, 7890–7896 **(2013)**.

[18] J.Z.Wang, L.Lu, M.Lotya, J.N.Coleman, S.L.Chou, H.K.Liu, A.I.Minett, J.Chen; "Development of MoS_2–CNT composite thin film from layered MoS_2 for lithium batteries", Advanced Energy Materials, **3(6)**, 798–805 **(2013)**.

[19] Y.T.Liu, X.D.Zhu, Z.Q.Duan, X.M.Xie; "Flexible and robust MoS_2–graphene hybrid paper cross-linked by a polymer ligand: A high-performance anode material for thin film lithium-ion batteries", Chemical Communications, **DOI:** 10.1039/C3CC45936E, **49(87)**, 10305–10307 **(2013)**.

[20] Y.Liu, W.Wang, Y.Wang, X.Peng; "Synergistic performance of porous laminated tungsten disulfide/copper oxide/single-wall carbon nanotubes hybrids for lithium ions batteries", *Electrochimica Acta*, **148**, 73–78 **(2014)**.

[21] H.Kaiya, S.Suzuki, M.Miyayama; *Key Engineering Materials*, **388**, 41-44 **(2009)**.

[22] K.Hirai, T.Ichitsubo, T.Uda, A.Miyazaki, S.Yagi, E.Matsubara; "Effects of volume strain due to Li–Sn compound formation on electrode potential in lithium-ion batteries" *Acta Materialia*, doi:10.1016/j.actamat.2007.12.002, **56(7)**, 1539–1545 **(2008)**.

[23] J.W.Wei, Z.W.Ma, H.Zeng, Z.Y.Wang, Q.Wei, P.Peng; "Electronic and optical properties of vacancy-doped WS_2 monolayers", *AIP ADVANCES*, **2**, 042141 **(2012)**.

[24] G.B.Mitra; *Acta Crystallo*, "Determination of particle size and strain in a distorted polycrystalline aggregate by the method of variance", DOI: 10.1107/

S0365110X6400192X, **17(6)**, 765-766 **(1964)**.

[25] G.B.Williamson, R.E.Smallman; "Dislocation densities in some annealed and cold-worked metals from measurements on the X-ray debye-scherrer spectrum", *Philoophicals Magazine*, DOI:10.1080/14786435608238074, **1**, 34-45 **(1956)**.

[26] JCPDS X-ray Powder Diffraction file, 841398, Hexagonal WS_2.

[27] JCPDS X-ray Powder Diffraction file, 080237, Hexagonal WS_2.

[28] B.F.Mentzen, M.J.Sienko; *Inorg Chem.*, **15**, 2195 **(1976)**.

[29] L.F.Schneemeyer, M.J.Sienko; "Crystal data for mixed-anion molybdenum dichalcogenides" *Inorg Chem.*, DOI: 10.1021/ic50205a047, **19(3)**, 789-791 **(1980)**.

[30] M.K.Agarwal, M.N.Vashi, A.R.Jani; "Growth and characterization of layer compounds in the series $WS_x Se_{2-x}$**"**, *J.Cryst.Growth,* **71(2)**, 415-420 **(1985)**.

[31] S.Bhattecharjee, G.D.Nigam; "Introduction to Crystal Lattice Defects", Pragati Prakashan, Meerut, India **(1990)**.

[32] W.E.Warren; X Ray measurement of stacking fault widths in FCC metals, "*Journal of Appied Phys*ics", doi.org/10.1063/1.1777086, **32(11)**, 428, **(1961)**.

[33] C.N.J.Wagner, A.S.Tetelman, M.H.Ottee; "Diffraction from layer faults in bcc and fcc Structure", *Journal of Appied Phys*ics, doi.org/10.1063/1.1728571, **33(10)**, 3080 **(1962)**.